J Fluoresc (2014) 24:951–958
DOI 10.1007/s10895-014-1378-z

ORIGINAL PAPER

Sugar Binding Effects on the Enzymatic Reaction and Conformation Near the Active Site of Pokeweed Antiviral Protein Revealed by Fluorescence Spectroscopy

Hiromichi Nakashima · Yukihiro Fukunaga · Ryosuke Ueno · Etsuko Nishimoto

Received: 25 December 2013 / Accepted: 19 March 2014 / Published online: 4 April 2014

Abstract In various trials for elucidating the physiological function of pokeweed antiviral protein (PAP), studies on the interaction with sugar are essential. The fluorescence titration curves showed that PAP retained the strong affinity against N-acetylglucosamine (NAG) and two sites in one PAP molecule co-operatively participated in the binding. In the complex of PAP with NAG, Trp208 located at the entrance lid site of substrate came closer to Tyr72 about 0.3 Å. Furthermore, the fluorescence anisotropy decay measurement demonstrated that the segmental rotation of Trp208 was enlarged by the binding of PAP with NAG. Such conformational changes around the active site closely correlate with the enzymatic activity of PAP. The N-glycosidase activity of PAP was enhanced more than two times in the presence of NAG. The obtained results consistently suggested the enzymatic activity of PAP would be regulated through the conformation change near the active site induced by the binding with NAG.

Keywords Ribosome-inactivating protein · Pokeweed anti-viral protein · N-glycosidase · FRET · Fluorescence depolarization

Abbreviations

PAP	Pokeweed anti-viral protein
RIP	Ribosome-inactivating protein
FRET	Fluorescence resonance energy transfer
NAG	N-acetylglucosamine
TCSPC	Time-correlated single photon counting

H. Nakashima · R. Ueno · E. Nishimoto (✉)
Institute of Biophysics, Faculty of Agriculture
Graduate School of Kyushu University,
Hakozaki, Higashi-ku, Fukuoka 812-8581, Japan
e-mail: enish@brs.kyushu-u.ac.jp

Y. Fukunaga
Institute of Material Chemistry and Engineering, Kyushu University,
Kasuga, Fukuoka 816-8580, Japan

Introduction

Ribosomal inactivating proteins (RIPs) play a role as the bio-defense relating protein in almost every herbicide [1–4]. RIPs is originally N-glycosidase and catalyzes the adenine moiety releasing reaction from r-RNA. Because of this enzymatic action of RIPs disturbs the transcription and inhibits the protein synthesis in various fungi, bacteria and virus. Pokeweed antiviral protein (PAP) belongs to RIPs family and exhibits the enzyme activity against DNA in addition to RNA, while it has very similar tertiary structure with other RIPs. The relationship between the inhibition of protein synthesis and enzymatic action of PAP has been established through many investigations using the ribosomes [5]. However, the enzymatic mechanism and other relating properties as N-glycosidase are remained unclear. While PAP is a potent protein for medical application because of the anti-viral and anti-cancerous actions, it is a suicide protein in the mother herbicide cell. Therefore, the elucidation of the regulation mechanism of PAP is essential as well as the enzymatic reaction mechanism. RIPs is generally classified into two classes, one is Type I and the other Type II. Type I is a single polypeptide exhibits the N-glycosidase and Type II is composed of two polypeptides which show sugar binding property (B-chain) and glycosidase activity (A-chain), respectively. Type II RIPs is considered to keep stronger anti-viral action because lectin chain displays the strong affinity to the sugars composing the cell wall of many micro-organisms. Not confirmed yet, it is reasonable to

assume that Type I RIPs keep the affinity against the sugar to enhance the physiological function. In the present studies, the binding of PAP with N-acetylglucosamine (NAG) was examined and the resulting effects on the enzyme activity and the conformation near the active site were investigated using fluorescence spectroscopic method.

Three dimensional structure of PAP was shown in Fig. 1. The active site is composed of Arg, Glu and Tyrs. Two Tyrs participate in the binding with the substrate, RNA to complete the catalytic reaction by Arg and Glu. Similarly with other RIPs, PAP arranges Trp208 at the position of the entrance lid of the active site. Trp208 is considered to play a critical role in the enzymatic action of RIPs and at the same time very useful probe for the conformational change near the active site induced by the interaction with sugar through the steady-state and time-resolved fluorescence methods. The advantage and validity of the fluorescence of tryptophan are well known in the studies on the protein structure, function and dynamics [6]. The potentiality of fluorescence of Trp208 was shown in the structural change during the folding/unfolding of PAP [7]. PAP includes another Trp residue, Trp237 at the C-terminal domain. Therefore, two mutant PAPs of which Trp237 and Trp208 were replaced with Phe, respectively were used in order to specify the fluorescence of each Trp and significance of Trp208 fulfill in the enzymatic reaction of PAP.

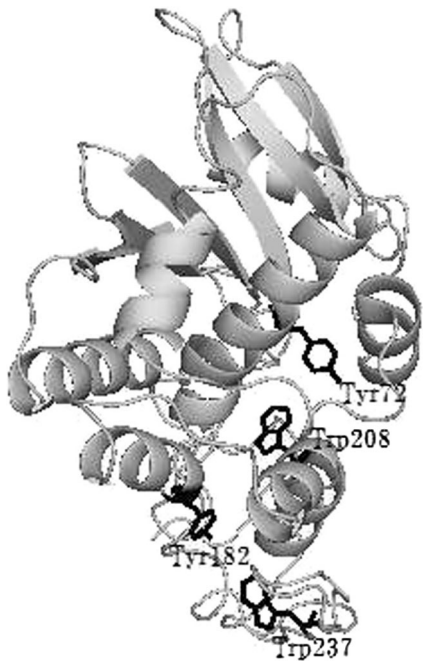

Fig. 1 The crystal structure of pokeweed anti-viral protein (PAP). The crystal structure of PAP was presented (PDB accession code 1PAF). Two tryptophan residues in PAP, Trp208 and Trp237 and nearest neighboring Tyr72 and Tyr182 were indicated by *thick line*. The X-ray structure was drawn by swiss-pdb viewer

Materials and Methods

Materials

*Eco*RI and *Bam*HI were purchased from Nippon Gene Co Ltd. (Tokyo, Japan) and New England Biolabs Inc. (Ipswich, MA), respectively. DNA polymerase, KOD-plus-Ver. 2 was a product of Toyobo (Osaka, Japan). Tryptone and yeast extract were purchased from Difco Laboratories (BD, Franklin Lakes, NJ). Factor Xa and Amylose resin for affinity column were purchased from Novagen (Merck KGaA, Darmstadt, Germany) and New England BioLabs Inc., respectively. Mono S 5/50 GL was obtained from GE Healthcare UK (Buckinghamshire, UK) and used for cation exchange column chromatography.

Expression and Purification of Recombinant PAP

The expression of PAP was performed as described previously [8], except that the expression vector pMALY-p2 was used instead of pMAL-p2 (New England BioLabs). The pMALY-p2 yeast/Escherichia coli shuttle vector was constructed by inserting a 2 μ yeast replication origin and a *URA3* selectable marker into pMAL-p2 as previously reported [9], and used for cloning and site-directed mutagenesis by in vivo homologous recombination in yeast [9, 10]. The DNA fragment encoding the mature region of PAP or its mutant was inserted between *Bam*HI and *Hin*dIII sites of pMALY-p2 and introduced into the *E. coli* strain XL1-Blue (Stratagene, CA). The transformant was grown at 37 °C in 1 l of LB medium containing ampicillin (100 μg/ml) and tetracycline (12 μg/ml) to an OD of 1.0 at 600 nm, and then incubated with 0.35 mM isopropyl-β-D- thiogalactopyranoside for 5 h at 25 °C to induce expression of the PAP fusion with maltose-binding protein (MBP-PAP). The MBP-PAP was extracted from periplasmic fractions of harvested bacterial cells into distilled water including 5 mM $MgSO_4$ in the ice bath. After removing the debris by centrifugation, the sample solution was adopted to amylose resin affinity column to separate PAP from other protein. The maltose binding protein was removed using Factor Xa in 50 mM Tri-HCl buffer (pH 8.0) including 0.1 M NaCl, 1 mM dithiothreitoland 5 mM $CaCl_2$. Wild type and mutant PAP were finally purified by Mono-S column using NaCl gradient from 0 to 0.3 M. Every chromatography was performed on Biologic DuoFlow System (BioRad, Hercules, CA). The purities of PAP were confirmed by SDS-PAGE.

Enzymatic Activity

The measurement of enzymatic activity of PAP was followed by Zamboni et al. [11]. Briefly, PAP was incubated at 40 °C for 1 h in the buffer solution including 50 μg of DNA of salmon sperm. The released adenine by the enzymatic reaction

of PAP was separated by ethanol precipitation and changed to 1,N^6-ethenoadenine by the reaction with chloroacetaldehyde. This fluorescent adenine derivative shows the absorption and fluorescence emission maxima at 310 and 410 nm, respectively. Therefore, measurement of the enzymatic activity of PAP was performed through the quantitative analysis of 1,N^6-ethenoadenine by fluorescence HPLC using excitation wavelength of 310 nm and emission wavelength of 410 nm.

Steady-State Fluorescence

The steady-state fluorescence spectrum was measured with HITACHI 3010 fluorescence spectrophotometer (Tokyo, Japan). The excitation/emission bandpath was 5/5 nm. The fluorescence emission spectrum was strictly corrected against the detection and excitation systems. The undesired effects caused by stray and scattering light were removed with subtraction method.

The binding properties of PAPs with NAG were investigated based on Hill plots,

$$\Delta F/F_0 = \frac{[\mathrm{NAG}]^n}{K_\mathrm{d} + [\mathrm{NAG}]^n} \tag{1}$$

where n was co-operative index, K_d dissociation constant and ΔF relative increment of the fluorescence intensity created by NAG and F_0 the fluorescence intensity in the absence of NAG. The estimation of ΔF was based on the fluorescence titrations. The fluorescence spectrum was measured in the buffer solution including various concentration of NAG with keeping PAP concentration constant. The fluorescence intensity at the maximum wavelength was used for the estimation of ΔF and F_0.

Fluorescence Intensity and Anisotropy Decay

The fluorescence intensity and anisotropy decay were measured by a sub-pico second laser based time correlated single photon counting (TCSPC) system. The excitation pulse of 285 and 295 nm were separated from a combination of sub-pico second pulse laser (TSUNAMI, Spectra-Physics, Mountain View, CA) synchronously pumped by green laser (Millenia XsJ, Spectra-Physics) with second harmonic generator/pulse selector (model 3980, Spectra-Physics) and third harmonic generator (GWU, Spectra-Physics). The fluorescence photon pulses were detected by a multi-channel plate type photomultiplier (3809U-50, Hamamatsu Photonics, Shizuoka, Japan) and fed into the start channel of a time-to-amplitude converter (TAC457, Ortec, Oak Ridge, TN) after the amplification by GHz AMP (model9327, Ortec). The stop signal for the time-to-amplitude convertor was obtained by detecting and amplifying the excitation pulse by APD (C5658, Hamamatsu Photonics). The output signal from TAC was stored in 2,048 channels of a multi-channel analyzer (Maestro-32, Ortec). The channel width was 8.54 ps. The fluorescence decay function was given by linear combination of some exponentials as Eq. 2,

$$F(t) = \sum \alpha_i \exp(-t/\tau_i) \tag{2}$$

where τ_i and α_i was the fluorescence decay time of i-th component and the corresponding pre-exponential factor. The decay kinetics and parameters were decided by convolution-nonlinear least square methods based on the Marquard argolism [12, 13]. Their adequacy was judged by the inspection of the residuals and statistical parameters such as sigma value (σ) and serial variance ratio (SVR).

The fluorescence anisotropy, r, was defined on Eq. 3.

$$r = \frac{I_{vv} - G I_{vh}}{I_{vv} + 2G I_{vh}} \tag{3}$$

I_{vv} and I_{vh} were the intensities of parallel and perpendicular component against the vertically polarized excitation, respectively. G was the grating factor. One Gran-Taylor polarizer was set vertical or horizontal at the emission side to measure I_{vv} and I_{vh}. G factor was decided by measuring the intensity ratio of I_{vv} to I_{vh} against the horizontal excitation.

The fluorescence anisotropy decay kinetics were given by

$$r(t) = \sum \beta_i \exp(-t/\tau_i) \tag{4}$$

where ϕ_i and β_i were the rotational correlation time of i-th component and the corresponding to the amplitude, respectively. The decay parameters were decided by the global analysis of I_{vv} and I_{vh}, since Eq. 5 are satisfied between the fluorescence intensity decay, $F(t)$, and anisotropy decay, $r(t)$.

$$I_{vv} = \frac{1}{3} F(t)[1 - r(t)], \quad I_{vh} = \frac{2}{3} F(t)[1 - 2r(t)] \tag{5}$$

The quality of the fitting was confirmed similarly with the fluoresecence intensity decay. The instrument and analyzing methods of TCSPC used here was reported in the previous paper in detail [14].

Results and Discussion

Binding of N-acetylglucosamine

The fluorescence spectra of WT- and mutant PAP were shown in Fig. 2. The fluorescence maximum wavelengths of W237F-, W208F- and WT-PAP were found at 335 nm, 350 nm and 345 nm, respectively to show that Trp208 located at the hydrophobic region and the circumstance surrounding Trp237 is hydrophilic. The fluorescence intensities of PAP were reduced by the additions of NAG without the spectral shift as shown in Fig. 3. It is clear that the decrease of fluorescence intensity by NAG is not due to the collision quenching but the binding since the quenching is induced by the NAG concentration of same order to PAP. The strong collisional quenching requires one or two order higher concentration of quencher like acrylamide. Since linear plots like the plot of Klotz did not show the consistent results between the fluorescence increment and the concentration of NAG, the relative increments of fluorescence intensity, $\Delta F/F_0$ was plotted against the NAG concentration based on the Hill equation (Eq. 1). As shown in Fig. 4, WT-, W237F- and W208F-PAP showed excellent fit for the binding with NAG (the results of W208F-PAP is not shown). The cooperativity index, n=1.47 and dissociation constant, K_d= 1.65 μM were estimated for WT-PAP. The biding parameters for the other two mutant PAPs were summarized in Table 1. The replacement of Trp208 or Trp237 with Phe gave large effects on the sugar binding properties of PAP. Although also two mutant PAPs retained strong affinity to NAG, the dissociation constant of W237F-PAP was increased and the cooperative index was decreased. This result suggests that Trp237 would participate in holding the structure for sugar binding. The replacement of Trp208 did not affect the dissociation constant but the cooperative index for the sugar binding. In this way, the replacement of two Trp residues changed the binding parameter. However, the binding stoichiometry of PAP and NAG was estimated to be 2 for every PAP because the initial increasing line and maximum line of $\Delta F/F_0$ intersected at the point indicating the ratio of [NAG]/[PAP] was 2 as shown in Fig. 4. (The result of W208F-PAP was not shown.) PAP retained two binding sites for NAG molecule regardless of the mutation.

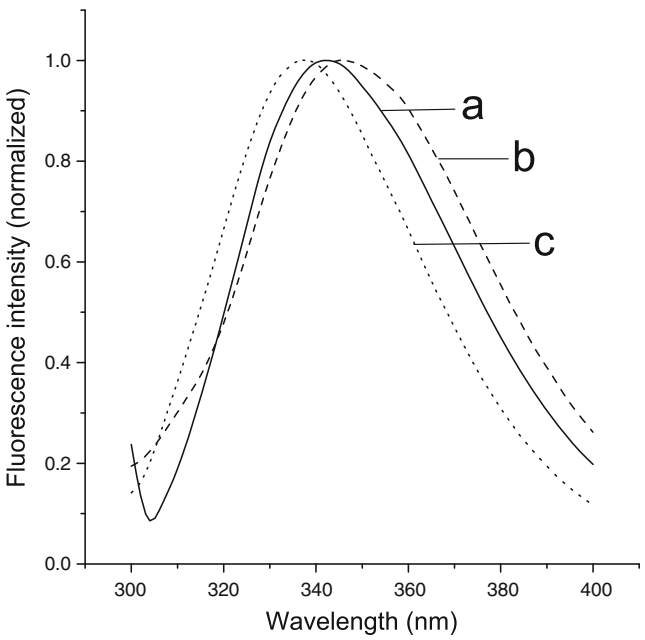

Fig. 2 Fluorescence spectra of PAPs. The excitation wavelength was 295 nm. Curves *a*, *b*, and *c* were spectra of WT-, W208F-, and W237F-PAP in 10 mM phosphate buffer (pH 6.5), respectively. The sample concentrations were adjusted OD_{280}=0.1

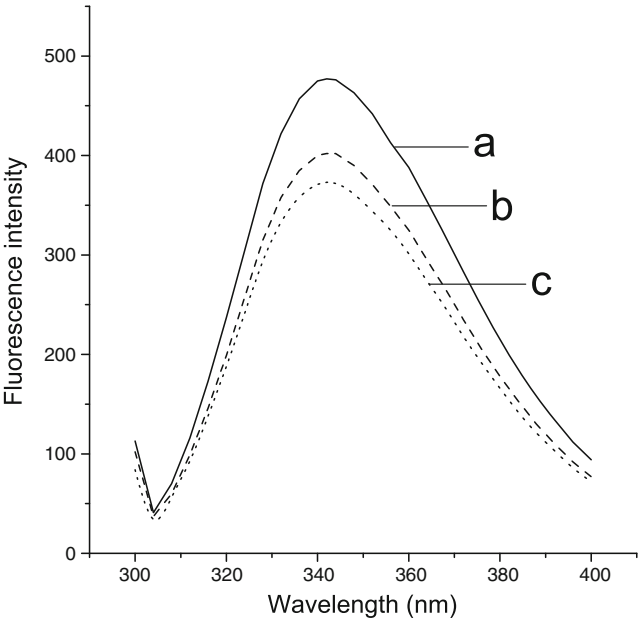

Fig. 3 NAG binding effects on the fluorescence spectrum of PAP. The excitation wavelength was 295 nm. The concentration of WT-PAP was 3 μM. The spectra of curves *a*, *b* and *c* contained 0, 4.5 and 11.7 μM of NAG in the 10 mM phosphate buffer (pH 6.5)

Binding Effects of NAG on the Enzymatic Activity

PAP exhibited the N-glycosidase activity on DNA. The enzymatic activity of PAPs was estimated by quantitative measurements of the released adenine from DNA. The results were shown in Fig. 5. The enzymatic activity of PAP was remarkably reduced by the replacement of Trp208 with Phe. The replacement of Trp237 rather increased the enzymatic activity of PAP. In the presence of NAG of which concentration was higher than 3 fold of one of PAP, the enzymatic activities of WT- and W237F-PAP were almost two times enhanced. Activity enhancement effect of NAG was not recognized in W208F-PAP. Although data were not shown, the enzymatic activities of WT- and W237F-PAP were increased with increase in the temperature but not W208F-PAP. These results reasonably concluded that W208 would be essential and

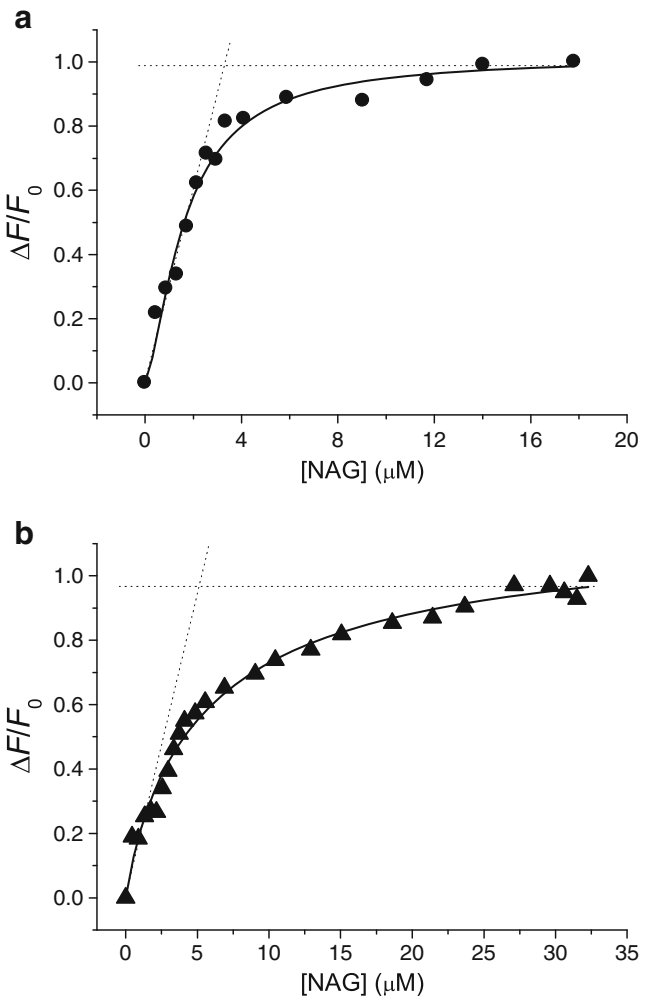

Fig. 4 Hill plots for the binding of WT- and W237F-PAP with NAG. Panel **a**, WT-PAP; Panel **b**, W237F-PAP. $\Delta F/F_0$ was plotted against NAG based on Hill equation (Eq. 1). F_0 was the fluorescence intensity in the absence of NAG and ΔF was estimated by the change in the fluorescence intensity by the binding with NAG. The concentrations of WT-PAP and W237F-PAP were 1.2 and 3.5 μM, respectively. *Two dot lines* drawn in Panel **a** and **b** indicate the initial increasing and the maximum of $\Delta F/F_0$, respectively

would play a critical role for the enzymatic activity because the activity enhancement effect was seen only in WT- and W237F-PAP.

Time-Resolved Fluorescence of PAP

The fluorescence intensity decay of W237F-PAP on the excitation at 285 nm was shown in Fig. 6. The fluorescence decays

Table 1 Binding parameters of PAPs with NAG

	n	K_d (μM)
WT	1.47	1.65
W208F	1.87	2.23
W237F	0.89	5.69

n cooperative index, K_d dissociation constant

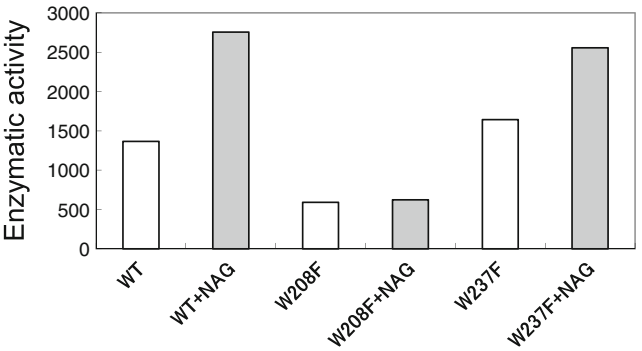

Fig. 5 NAG binding effect on N-glycosidase activity of PAPs. The enzymatic activity was given by the band intensity on the fluorescence HPLC corresponding to the adenine derivative. Concentrations of PAPs, DNA and NAG were 300 μM, 50 μg/80 μL and 750 μM, respectively. Reaction time was 60 min and temperature was 40 °C

of PAP showed peculiar dependence on the excitation wavelength. The fluorescence decay profile showed the specific round form on the excitation at 285 nm. On the other hand, on the excitation at 295 nm usual monotonous decay profile was observed. While the fluorescence decay kinetics was generally described with the linear combination of some exponential functions (Eq. 2), the decay curve with round form requires the negative pre-exponential factor for the adequate fit. The fluorescence decay parameters of the mutant PAP were summarized in Table 2. In the fluorescence intensity decay of Trp208, the pre-exponential factor corresponding to the fastest

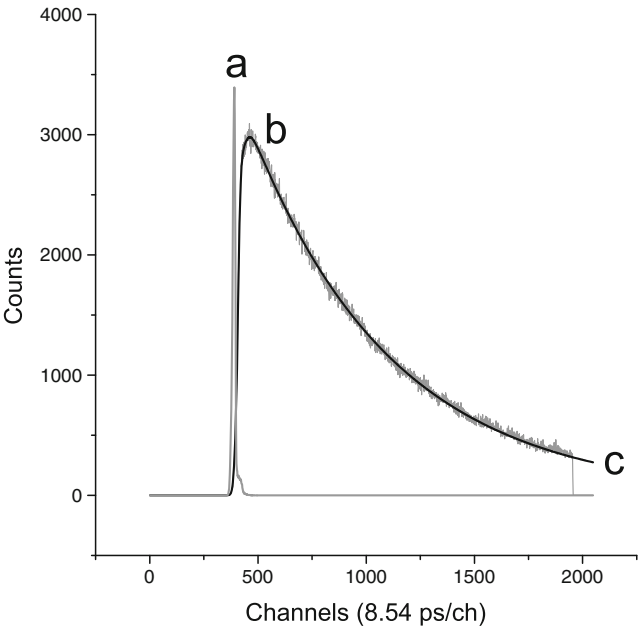

Fig. 6 Fluorescence intensity decay profile of W237F-PAP on the excitation at 285 nm. Curve *a* and *b* were the instrumental response function (IRF) and the fluorescence decay of W237F-PAP, respectively. Curve *c* was the decay curve described by using the parameters giving the best fit. The emission wavelength was 340 nm. Channel width, 8.54 ps/channel. The sample concentration was 5 μM

Table 2 The fluorescence decay parameters of W208F- and W237F-PAP on the excitation at 285 nm

	α_1	α_2	α_3	τ_1(ns)	τ_2(ns)	τ_3(ns)	σ	SVR
W208F	1.04	0.05	−0.09	6.60	1.36	0.22	1.07	1.74
W208F + NAG	1.00	–	–	6.46	–	–	1.03	1.98
W237F	1.10	−0.10	–	5.70	0.21	–	1.08	1.83
W237F + NAG	1.20	−0.18	–	5.60	0.18	–	1.05	1.82

decay time was negative. The excitation wavelength dependence and negative pre-exponential factor of fluorescence decay of PAP was rationalized by the resonance excitation energy transfer from Tyr to Trp because both of Trp and Tyr are excited at 285 nm but only Trp is excited exclusively excited at 295 nm. According to the simple kinetics for the electronic relaxation including the energy transfer process, the fluorescence decay kinetics of Trp is described Eq. 6,

$$F(t) = \frac{k_t D_0}{{}^1/_{\tau_D} - {}^1/_{\tau_A}} \left\{ \exp\left(-{}^t/_{\tau_D}\right) - \exp\left(-{}^t/_{\tau_A}\right) \right\} + A_0 \exp\left(-{}^t/_{\tau_A}\right) \quad (6)$$

where τ_A and τ_D are fluorescence lifetimes of the energy acceptor and donor, respectively, k_t the energy transfer rate constant and D_0 and A_0 are constants relating to the absorption of the donor and acceptor. As clearly shown in Eq. 6, the decay time corresponding to the negative pre-exponential factor is one of donor (nearest neighboring Tyr). Therefore, the energy transfer rate (k_t) is estimated by the experimentally decided decay time and the lifetime of Tyr without the energy acceptor using the relation given by Eq. 7,

$${}^1/_{\tau_D} - {}^1/_{\tau_D^0} = k_t \quad (7)$$

where, τ_D and τ_D^0 are the decay times of Tyr in the presence and absence of acceptor. The former was determined by the fluorescence decay of mutant PAP. The energy transfer rate is furthermore related with the energy transfer distance using the critical distance for the energy transfer between Tyr and Trp,

$$k_t = \frac{1}{\tau_D^0} \left(\frac{R_0}{R} \right)^6 \quad (8)$$

where R_0 is the critical distance and R is the energy transfer distance [15]. Using 3.14 ns [16] and 14 Å [17] for τ_D^0 and R_0 of which validities were confirmed in some reports [18], the changes in the energy transfer distance of PAP by the binding with NAG were estimated. The results were summarized in Table 3. The change in the energy transfer distance between Trp208 and the nearest neighboring Tyr corresponded to Tyr72 in this case was estimated to be small (0.3 Å) but substantially shrunk in W237F-PAP by the binding of NAG. Trp237 locates in C-terminal domain and adjacent with Tyr182 in the N-terminal domain. When W208F-PAP bound with NAG, the fluorescence decay kinetics switched to the single exponential giving no negative pre-exponential factor. This result suggests that the distance between Trp237 and

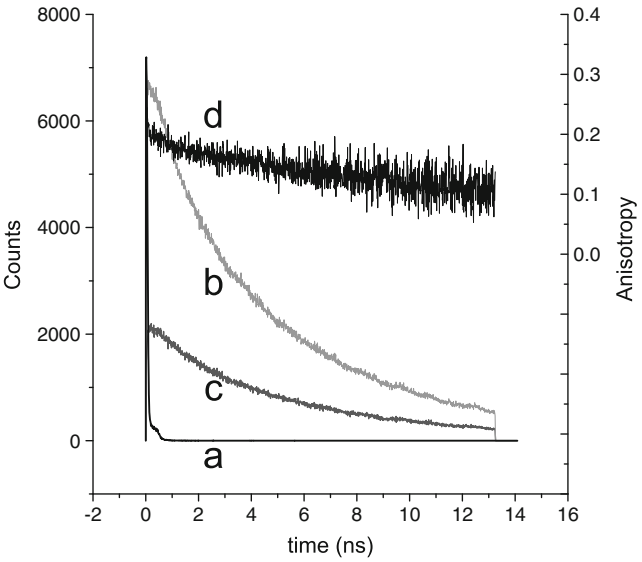

Fig. 7 Fluorescence anisotropy decay of W237F-PAP. Curve *a*, instrumental response function; Curve *b* and *c*, I_{vv} and I_{vh}; Curve *d*, fluorescence anisotropy decay of W237F-PAP. I_{vv} and I_{vh} were the decay of the vertically and horizontally polarized component against the excitation with vertically polarized laser pulse. Curve *d* was calculated using I_{vv} and I_{vh} based on the definition of fluorescence anisotropy. Excitation wavelength, 295 nm; Emission wavelength, 340 nm; The sample concentration was 5 μM

Table 3 Energy transfer distance between Trp and nearest neighbouring Tyr

Critical distance, 14 Å [17]; lifetime of donor without accepter, 3.14 ns [16]

	k_t (ns^{-1})	r (Å)
W237F-PAP	4.44	9.2
W237F-PAP + NAG	5.23	8.9
W208F-PAP	4.22	9.3
W208F-PAP + NAG	–	>28

Table 4 The fluorescence anisotropy decay parameters of W237F-PAP

	β_1	β_2	ϕ_1(ps)	ϕ_2(ns)	f
W237F	0.02	0.23	90	10.7	0.08
W237F + NAG	0.09	0.12	80	9.7	0.43

Tyr182 would be expanded more than 28 Å at least by the binding with NAG. Probably, such large conformation change near Trp237 by NAG did not directly involve in the enzymatic activity because the activity enhancement was not found in W208F-PAP. According to X-ray crystallographic structure of PAP, Tyr72 compose of the active site locates apart 9 Å from Trp28 with the most proximity. The results obtained here demonstrated that the distance between Tyr72 and Trp208 would be 9.2 Å. These two values are consistent and our estimation of the distance between Trp and Tyr would be reasonable even within the approximation for the orientation factor.

The measurement of fluorescence anisotropy decay of Trp208 would be important to describe the conformational change near the active site induced by the binding with NAG. The fluorescence anisotropy decay of W237F-PAP was shown in Fig. 7 and the decay parameters were summarized in Table 4 together with the results of the NAG binding effect. The fluorescence anisotropy decay kinetics was described with double exponential regardless of the binding with NAG. The longer rotational correlation time was almost 10 ns and the shorter 80–90 ps. These correlation times correspond to the entire rotation of PAP and segmental one of Trp208, respectively. The shorter correlation time became shorter by the binding with NAG. This result suggests that the segmental rotation of Trp208 would be free. The motional freedom (*f*) of Trp208 which is defined as

$$f = \frac{\beta_1}{\beta_1 + \beta_2}$$

where β_1 and β_2 correspond to the pre-exponential factor of the shorter and longer decay component, respectively, more clearly revealed the conformational change near the active site by the binding with NAG [19, 20]. The motional freedom was remarkably increased from 0.08 to 0.43. The shortening of the rotational correlation time and increasing in the motional freedom demonstrated that the segmental motion of Trp208 would be liberated near the active site by the binding of NAG.

Conclusion

PAP belongs to Type I RIPs and therefore not equip the lectin chain. However the affinity with sugar might be essential for PAP to complete the bio-defending role. The fluorescence titration studies of PAP demonstrated that two binding sites cooperatively participated in the binding with NAG although the binding parameters such as the dissociation constant and cooperative index were modified by the replacement of Trp208 or Trp237 with Phe. The enzymatic activity of W208F-PAP was much lower than those of WT- or W237F-PAP and not affected by the binding of NAG. On the other hand, the enzymatic activities of WT- or W237F-PAP were greatly enhanced in the presence of NAG. These experimental results demonstrate that Trp208 would play critical role in the N-glycosidase activity of PAP and the conformation surrounding Trp208 was altered by the binding of NAG. The time-resolved fluorescence studies showed that the segmental motion of Trp208 was liberated from the interaction with the surroundings with approaching closer a little to Tyr72 to enhance the enzymatic activity. If the binding site for NAG is specified, the acceleration mechanism by sugar could be described more precisely. Unfortunately, the binding site of NAG was not specified in the present work.

References

1. Au TK, Collins RA, Lam TL, Ng TB, Fong WP, Wan DCC (2000) The plant ribosome inactivating proteins luffin and saporin are potent inhibitors of HIV-1 integrase. FEBS Lett 471:169–172
2. Wang Y-X, Jacob J, Wingfield PT, Palmer I, Stahl SJ, Kaufman JD, Huang PL, Lee-Huang P, Lee-Huang S, Torchia DA (2000) Anti-HIV and anti-tumor protein MAP30, a 30 kDa single-strand type-I RIP, shares similar secondary structure and β-sheet topology with the A chain of ricin, a type-II RIP. Protein Sci 9:138–144
3. Corrado G, Bovi PD, Ciliento R, Gaudio L, Di Maro A, Aceto S, Lorito M, Rao R (2005) Inducible expression of a *Phytolacca heterotepala* ribosome-inactivating protein leads to enhanced resistance against major fungal pathogens in tobacco. Phytopathology 95:206–215
4. Park S-W, Stevens NM, Vivanco JM (2002) Enzymatic specificity of three ribosome-inactivating proteins against fungal ribosomes, and correlation with antifungal activity. Planta 216:227–234
5. Baykal U, Tumer NE (2007) The C-terminus of pokeweed antiviral protein has distinct roles in transport to the cytosol, ribosome depurination and cytotoxicity. Plant J 49:995–1007
6. Royer CA (2006) Probing protein folding and conformational transitions with fluorescence. Chem Rev 106:1769–1784
7. Matsumoto S, Taniguchi Y, Fukunaga Y, Nakashima H, Watanabe K, Yamashita S, Nishimoto E (2013) Structural characteristic of folding/unfolding intermediate of pokeweed anti-viral protein revealed by time-resolved fluorescence. J Fluoresc 23:407–415
8. Honjo E, Watanabe K (1999) Expression of mature pokeweed antiviral protein with or without C-terminal extrapeptide in *Escherichia coli* as a fusion with maltose-binding protein. Biosci Biotechnol Biochem 63:1291–1294
9. Iizasa E, Nagano Y (2006) Highly efficient yeast-based in vivo DNA cloning of multiple DNA fragments and the simultaneous construction of yeast/*Escherichia coli* shuttle vectors. BioTechniques 40:79–83
10. Marykwas DL, Passmore SE (1995) Mapping by multifragment cloning in vivo. Proc Natl Acad Sci U S A 92:11701–11705
11. Zamboni M, Brigotti M, Rambelli F, Montanaro L, Sperti S (1989) High-pressure-liquid-chromatographic and fluorimetric methods for the determination of adenine released from ribosomes by ricin and gelonin. Biochem J 259:639–643
12. Willis KJ, Szabo AG (1989) Resolution of tyrosyl and tryptophyl fluorescence emission from subtilisins. Biochemistry 28:4902–4908
13. Zuker M, Szabo AG, Bramall L, Krajcarski DT, Selinger B (1985) Delta function convolution method (DFCM) for fluorescence decay experiments. Rev Sci Instrum 56:14–22

14. Otosu T, Nishimoto E, Yamashita S (2009) Fluorescence decay characteristics of indole compounds revealed by time-resolved area-normalized emission spectroscopy. J Phys Chem A 113:2847–2853
15. Lakowicz JR (2006) Principles of fluorescence spectroscopy. Springer, New York
16. Lakowicz JR, Laczko G, Gryczynski I (1987) Picosecond resolution of tyrosine fluorescence and anisotropy decays by 2-GHz frequency-domain fluorometry. Biochemistry 26:82–90
17. Eisinger J, Feuer B, Lamola AA (1969) Intramolecular singlet excitation transfer. Applications to polypeptides. Biochemistry 8:3908–3915
18. Oishi O, Yamashita S, Nishimoto E, Lee S, Sugihara G, Ohno M (1997) Conformations and orientations of aromatic amino acid residues of tachyplesin I in phospholipid membranes. Biochemistry 36: 4352–4359
19. Lipari G, Szabo A (1982) Model-free approach to the interpretation of nuclear magnetic resonance relaxation in macromolecules. 2. Analysis of experimental results. J Am Chem Soc 104:4559–4570
20. Nishimoto E, Yamashita S, Szabo AG, Imoto T (1998) Internal motion of lysozyme studied by time-resolved fluorescence depolarization of tryptophan residues. Biochemistry 37:5599–5607